

Effect of multiple light paths on retinal vessel oximetry

Matthew H. Smith, Kurt R. Denninghoff, Arthur Lompado, and Lloyd W. Hillman

Techniques for noninvasively measuring the oxygen saturation of blood in retinal arteries and veins are reported in the literature, but none have been sufficiently accurate and reliable for clinical use. Addressing the need for increased accuracy, we present a series of oximetric equations that explicitly consider the effects of backscattering by red blood cells and lateral diffusion of light in the ocular fundus. The equations are derived for the specific geometry of a scanning-beam retinal vessel oximeter; however, the results should also be applicable to photographic oximeters. We present *in vitro* and *in vivo* data that suggest the validity of these equations. © 2000 Optical Society of America

OCIS codes: 170.0170, 170.1470, 170.3660, 170.4460, 170.6510.

1. Introduction

The arteries and veins of the retina are directly observable through the pupil of the eye. This optical accessibility of these vessels has prompted several investigations into noninvasive spectroscopic measurements of the oxygen saturation of the blood within the vessels.^{1–9} Each of the reported investigations into retinal vessel oximetry determines the oxygen saturation of blood within a retinal vessel by spectroscopic oximetry.¹⁰ Proposed diagnostic applications of retinal vessel oxygen saturation measurements range from monitoring glaucoma and diabetic retinopathy to noninvasively indicating blood loss in trauma victims.

The first retinal oximetry experiments, reported by Hickam *et al.* in 1963, used two different wavelength combinations.¹ Broadband (>100 nm FWHM) Wratten filters centered at 800 and 640 nm were used in a red–infrared instrument. A red–green instrument used interference filters (10 nm FWHM) centered at 640 and 510 nm. Both instruments were fundus cameras modified to take dual, quasi-monochromatic retinal photographs. Optical densities of the vessels were measured through manual analysis of the exposed film.

Cohen and Laing² reported a similar instrument in 1976. This instrument employed a blue–green combination, using interference filters (20 nm FWHM) centered at 470 and 515 nm. The multiple-scattering theory of Twersky¹¹ was used to explain their experimentally determined calibration curve.

In 1988, Delori³ reported a three-wavelength retinal vessel oximeter. This device scanned a slit of filtered light across the retina and automatically interpreted collected data by a computer algorithm. Three closely spaced green wavelengths (558, 569, and 586 nm) were chosen for this measurement so that the constant-scattering approximation of Pittman and Duling¹² could be applied.

Schweitzer *et al.*⁴ demonstrated a retinal imaging spectrometer in 1995. This technique is unique in that it determines retinal vessel oxygen saturation by transmittance measurements made at 2-nm increments from 400 to 700 nm. An empirical model of the wavelength dependence of scattering losses by red blood cells is also presented.

A recent photographic retinal oximeter was described in 1998 by Tiedeman *et al.*⁷ This instrument illuminates the retina with filtered light (8 nm FWHM) at 569 and 600 nm and acquires images on a high-dynamic-range CCD camera. These investigators have quantified the influence of retinal pigmentation on the calibration of their technique.⁹

Finally, Denninghoff *et al.*⁵ and Smith *et al.*⁶ described in 1997 and 1998, respectively, the first oximeter to focus lasers onto a subject's retina and scan the beams across a retinal vessel. Initial studies at two wavelengths (670 and 803 nm) showed significant variations in calibration between subjects. Recent *in vitro* studies¹³ at four wavelengths (629, 678, 821, and 899 nm) attained an excellent calibra-

M. H. Smith (SmithMH@email.uah.edu), A. Lompado, and L. W. Hillman are with the Department of Physics, University of Alabama, Huntsville, Alabama 35899. K. R. Denninghoff is with the Department of Emergency Medicine, University of Alabama, Birmingham, Alabama 35294.

Received 8 July 1999; revised manuscript received 16 November 1999.

0003-6935/00/071183-11\$15.00/0

© 2000 Optical Society of America

tion in a model eye by identifying a scattering wavelength dependence of blood. We show in this paper, however, that this wavelength-dependent scattering model does accurately describe measurements made *in vivo*.

Despite the scientific and engineering advancements made by each of these investigators, making highly accurate and reliable retinal saturation measurements remains an elusive goal. We are unaware of any devices that have been definitively shown to measure retinal oxygen saturation independent of vessel diameter, hemoglobin concentration, and fundus pigmentation.

One of the confounding aspects of whole-blood spectroscopic oximetry techniques is the scattering of light caused by the refractive-index discontinuity between red blood cells and the plasma in which they are suspended.^{14–16} Although most recent attempts at retinal vessel oximetry have employed some sort of scattering compensation, in this paper we broaden the analysis of these scattering effects.

We also describe another effect that complicates retinal vessel oximetry. This effect is the lateral diffusion of light in the layers of the ocular fundus that lie beneath the retinal vasculature. As a result of this diffusion, a fraction of the light detected by a retinal oximeter has undergone a single absorption pass through the blood vessel, and a portion of the light has undergone a double pass. We refer to this mixture of single-pass and double-pass light as multipass transmission. Most previous retinal oximetry investigations mention this effect, but in this paper we provide a more detailed mathematical treatment.

By examining all the light paths that comprise a retinal vessel oxygen saturation measurement, we derive an oximetry equation that accounts for both scattering and multipass effects. Unfortunately, it is difficult to calculate oxygen saturation with this equation because of the large number of unknown parameters. To overcome this difficulty, we present a number of approximations to the oximetry equation that allow the calculation of oxygen saturation under certain simplifying approximations. Finally, we present *in vivo* data acquired in swine and *in vitro* data acquired in a model eye that indicate the utility of these equations.

2. Light Paths in Retinal Vessel Oximetry

There are two optical techniques that have been used to spectroscopically determine the oxygen saturation of blood in retinal vessels. In the first method, an area of the retina is illuminated and retinal images are formed on film or on a CCD detector array. These retinal images are acquired at multiple wavelengths. In the second method, multiple monochromatic beams are scanned across a retinal vessel, and the light that reflects back out of the eye is collected at discrete points along the scan. In both methods, the reflected light from the center of the vessel is compared with the reflected light from the fundus on each side of the vessel to calculate the transmittance of the blood within the vessel. An oximetric equa-

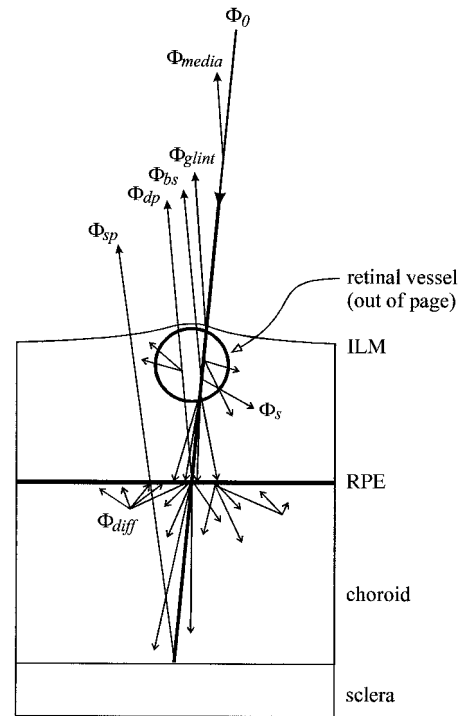


Fig. 1. Primary light paths associated with a scanning-beam retinal vessel oximetry measurement; Φ_0 , incident light; Φ_{media} , scattered light from the lens and vitreous; Φ_{glint} , specular reflection from the inner limiting membrane (ILM) or vessel wall; Φ_s , light scattered away by red blood cells (RBC's) within the vessel; Φ_{bs} , light backscattered to the detector by RBC's; Φ_{sp} , light collected that has traversed the vessel in single pass; Φ_{dp} , light collected that has traversed the vessel in double pass; Φ_{diff} , light diffused laterally in the choroid; RPE, retinal pigment epithelium.

tion is used to calculate oxygen saturation from the transmittance measurements made at multiple wavelengths. The discussions that follow are derived for a scanning retinal vessel oximeter system; however, all the results should be applicable to an imaging system.

Figure 1 illustrates the primary light paths in retinal vessel oximetry. A beam of light with flux Φ_0 is directed into the pupil of the eye and is focused onto a retinal vessel. A retinal vessel oximeter system then collects the fraction of light that is reflected back out of the pupil of the eye. There are several light paths that contribute to this collected power. First, some quantity Φ_{media} of the incident flux may directly backscatter from the lens or vitreous and be collected. Next, there is a specular reflection from the apex of the vessel, Φ_{glint} , that may exit the pupil and be collected. This reflection may originate from the inner limiting membrane¹⁷ (ILM) or from the vessel wall, but any portion of this glint that is caused by backscattering from blood within the vessel is considered in a separate term, Φ_{bs} , below. As the incident beam propagates through the blood within the vessel, the flux of the beam is decreased by the Lambert–Beer law because of absorption by hemoglobin and oxyhemoglobin within the red blood cells (RBC's). In ad-

dition, light is scattered by the RBC's. Some quantity of this scattered light Φ_s is scattered into angles that cannot be collected by the instrument, causing an apparent increase in absorption. There is another quantity of light, Φ_{bs} , that is directly back-scattered toward the instrument, resulting in an apparent decrease in absorption.

The beam that emerges from the other side of the vessel is enlarged because of scattering and attenuated because of absorption. The beam traverses the transparent rods and cones of the retina and finally reaches the scattering layers of the retinal pigment epithelium (RPE) and choroidal plexus that are ~ 240 μm posterior to the vessel.¹⁸ Strong melanin and hemoglobin absorption limits lateral diffusion and results in a tightly localized point spread function (PSF) on the RPE for visible wavelengths shorter than 575 nm. Wavelengths much longer than 575 nm penetrate the choroid deeply, reflecting off of the sclera and passing back through the choroid. As a result, the laterally diffused PSF of these longer wavelengths is much larger than that of shorter wavelengths. Reasonable estimates for the width (twice the standard deviation) of the diffusion-enlarged PSF in the nasal fundus (near the optic nerve head) have been reported to be ~ 60 μm from 450 to 575 nm and ~ 150 μm from 600 to 750 nm.¹⁹ A fraction of the light, Φ_{dp} , within this diffused PSF will pass back through the vessel to be absorbed and scattered in double pass and then exit the pupil of the eye. In addition, a fraction, Φ_{sp} , will extend beyond the edge of the vessel and exit the pupil of the eye in a single pass. Note that this geometry illustrated in Fig. 1 is specific to a scanning-beam oximeter. In a photographic oximeter geometry, the single-pass component Φ_{sp} would be incident on the fundus lateral to the vessel and reflect out of the eye through the vessel. The resulting equations derived in Section 3, however, should remain the same.

Figure 2, drawn to scale, demonstrates the likely existence of both single-pass and double-pass components of collected light. A 100- μm retinal vessel positioned 240 μm anterior to the reflecting layers of the ocular fundus is considered. Two separate diffusion-enlarged PSF's are considered, a 60- μm (twice the standard deviation) PSF typical of blue wavelengths and a 150- μm PSF typical of red and near-infrared wavelengths. Finally, 10° cones of light are illustrated that indicate the acceptance angle of an ~ 4 -mm-diameter pupil located 22 mm away. Thus only light in this solid angle can be collected by a retinal vessel oximeter. It is clear from this illustration that both single-pass and double-pass absorption need to be considered for typical retinal geometries. The relative magnitudes of these components depend on numerous factors including the PSF size, the diameter of the pupil, the vessel diameter, and the specular and diffuse reflectance properties of the ocular fundus. The relative magnitudes of single-pass and double-pass transmission are also acutely dependent on the specific geometry of the oximeter apparatus. A Monte Carlo simulation of

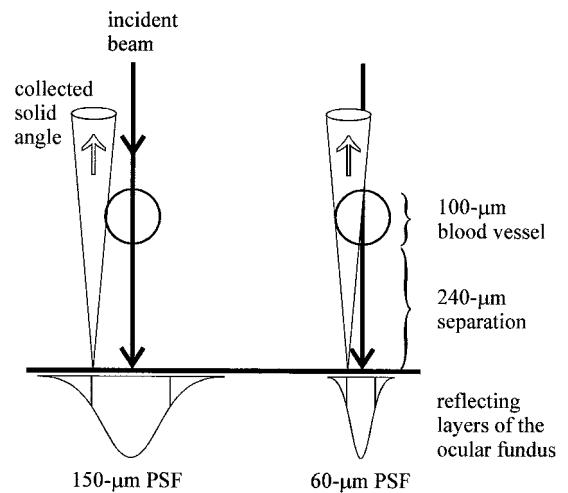


Fig. 2. Laser light traverses a retinal blood vessel and diffuses laterally in the reflecting layers of the ocular fundus. The diameter of the diffusion-enlarged PSF varies with wavelength, and two typical PSF diameters are illustrated. Only light that scatters into the indicated solid angle exits back out of the eye. The larger PSF demonstrates both single-pass and double-pass transmission through the vessel, whereas the smaller PSF demonstrates primarily single-pass transmittance.

retinal vessel profiles performed by Hammer *et al.*²⁰ predicts that the single-pass, double-pass, and back-scattered components contribute nearly equally for a 100- μm vessel. Single-pass light dominates for smaller (25- μm) vessels, and backscattered light dominates for larger (200- μm) vessels.

3. Oximetry Equations

A. Traditional Oximetry Equation

To date, all attempts at retinal vessel oximetry have employed some form of the equation

$$T_v(\lambda) = T_s(\lambda)\exp[-\varepsilon(\lambda)\chi cd], \quad (1)$$

where

$$\varepsilon(\lambda) = s\varepsilon_{\text{HbO}_2}(\lambda) + (1 - s)\varepsilon_{\text{Hb}}(\lambda). \quad (2)$$

In Eq. (1), $T_v(\lambda)$ is the measured transmittance of a retinal vessel at wavelength λ . This transmittance is calculated by one dividing the collected flux from the center of a vessel Φ_v by the flux collected from the fundus on either side of the vessel Φ_f . A typical technique for measuring T_v is illustrated in Fig. 3. The exponential term of Eq. (1) is simply the Lambert-Beer law describing the absorption of light by the blood within the vessel, where s is the oxygen saturation, c is the hemoglobin concentration, and d is the diameter of the vessel (i.e., the path length through the vessel). The absorption coefficients $\varepsilon_{\text{Hb}}(\lambda)$ and $\varepsilon_{\text{HbO}_2}(\lambda)$ of hemoglobin and oxyhemoglobin, respectively, are well-known functions of wavelength.^{10,21} The scattering effects of RBC's are described by the transmittance factor $T_s(\lambda)$. This factor represents light that has been scattered into angles that are not collected by the retinal oximeter.

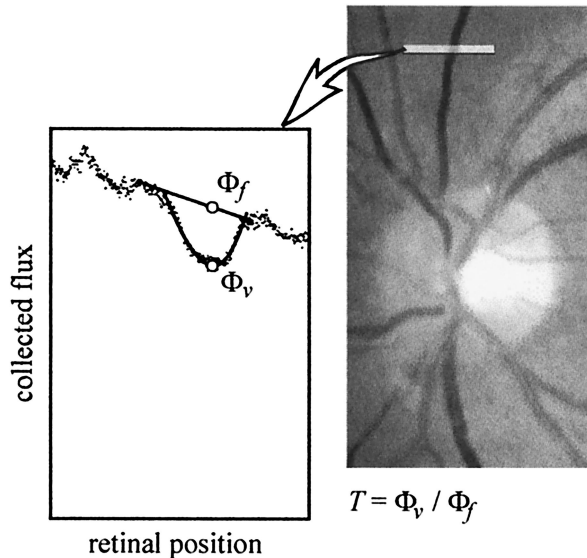


Fig. 3. Typical vessel absorption profile. The vessel transmittance T_v is calculated as Φ_v/Φ_f where Φ_v is the collected flux from the center of the vessel and Φ_f is an estimate of the flux that would be collected from the ocular fundus in the absence of the retinal vessel (estimated here by a linear approximation).

These photons are lost, resulting in an apparent increase in the vessel absorption (i.e., decreased transmittance). Some of the scattering factors that have been used include constants,³ linear functions,¹³ and empirical functions of wavelength.⁴ A geometry-dependent correction factor χ can be included in the absorption term. By measuring $T_v(\lambda)$ at multiple wavelengths, values of s , $T_s(\lambda)$, and the χcd product can be directly calculated or determined by a least-squares regression.

The parameter χ in Eq. (1) warrants further consideration. If all the light collected by a retinal oximeter traversed the blood vessel in double pass, then χ would equal 2. Similarly, if all the collected light traversed the vessel in single pass, then χ would equal 1. It is tempting to assume that χ would simply take on a value between 1 and 2 for the case of multipass transmission and that this value would be absorbed into the χcd product. However, as shown in Subsection 3.B, this assumption is not accurate.

B. General Multipass Transmittance Oximetry Equation

We derive an oximetry equation based on the light paths described in Fig. 1. As illustrated in Fig. 3, the transmittance T_v of a retinal vessel is defined as the ratio

$$T_v = \frac{\Phi_v}{\Phi_f}, \quad (3)$$

where Φ_v is the measured flux from the center of a vessel and Φ_f is the measured flux from the ocular fundus on either side of the vessel. The flux reflected from the fundus can be expressed simply as

$$\Phi_f = R_f \Phi_0, \quad (4)$$

where Φ_0 is the incident flux and the reflectance of the fundus R_f can encompass numerous factors such as the transmittance of the ocular media, the spectral characteristics of the absorbing layers of the ocular fundus, and the diameter of the exit pupil of the eye. Note that Φ_f cannot be measured directly, and its value must be interpolated from reflectance measurements on either side of the vessel. In practice, the data used to determine Φ_f must be measured sufficiently far from the vessel that the diffusion-enlarged PSF does not interact with the vessel causing a decreased background measurement.

To determine the flux collected from the center of a vessel Φ_v , consider all the light paths in Fig. 1 that can exit back out of the eye and be detected by the oximeter instrumentation. A summation of these light paths yields the expression

$$\Phi_v = \Phi_{sp} + \Phi_{dp} + \Phi_{bs}, \quad (5)$$

where Φ_{sp} is light that traversed the vessel in a single pass, Φ_{dp} traversed the vessel in a double pass, and Φ_{bs} is light that has been directly backscattered by the blood.

The single-pass and double-pass absorption components can be expressed by the Lambert–Beer law, resulting in

$$\Phi_v = \alpha R_f \Phi_0 \exp(-\epsilon cd) + \beta R_f \Phi_0 \exp(-2\epsilon cd) + \Phi_{bs}. \quad (6)$$

The absorption coefficient ϵ is defined by Eq. (2), and the wavelength dependence of ϵ still exists but is no longer stated explicitly. The coefficients α and β are the fractions of light transmitted in single pass and double pass, respectively.

It is important to note that a series of approximations were made in the derivations of Eqs. (4) and (6). First, we neglected Φ_{media} as a collected light path. A confocal optical system will prevent light backscattered from the lens and vitreous from reaching the detector. For photographic systems and nonconfocal scanning systems, however, it is not clear that this backscattered light will be negligible. Future studies should address this effect. In addition, we assume that Φ_{glint} will be prevented from affecting the measurement. Several techniques for eliminating the effects of the glint have been proposed; portions of the vessel lateral to the glint can be used for analysis,^{3,9} areas along the vessel that are free of glints can be used,¹ or curve fitting to the vessel profile can estimate the transmittance in the absence of the glint.⁶ We found that illuminating the eye with vertically polarized light and collecting only horizontally polarized light nearly eliminates the glint in scans acquired from a human eye. Although the crossed polarizers result in significantly reduced signals, high-quality scans that are free of glints (such as the scan in Fig. 3) can be easily obtained. Also note that any flux scattered out of the incident beam by the lens or vitreous and any light reflected out of the incident beam by the ILM or vessel wall should be

subtracted out of Φ_0 in Eqs. (4) and (6). We assume that these scattering and reflection losses are the same at the vessel and lateral to the vessel, and we choose to retain the term Φ_0 to reduce complexity and avoid confusion. Finally, note that the double-pass component of this expression is an approximation caused by the elliptical cross section of retinal vessels.

The scattering properties of samples of whole blood have been studied extensively,^{22,23} and several techniques^{24–26} have been used to predict these scattering properties. An important result of these studies is the relationship between the transmitted and the reflected (i.e., backscattered) portions of light incident on a sample of whole blood. Anderson and Sekelj²³ experimentally determined that the reflectance R of a blood sample is linearly related to the sample transmittance T , resulting in the equation

$$R = a_1 + a_2 \exp(-\epsilon cd). \quad (7)$$

Here, a_1 and a_2 are critically dependent on the sample hematocrit (i.e., the volume fraction of RBC's in whole blood) and the geometries of the source, detector, and sample. However, neither a_1 nor a_2 depend on the oxygen saturation of the sample. The experimental data supporting Eq. (7) were acquired between 600 and 630 nm, and the reflectance R refers to the light reflected into the entire back hemisphere from a planar sample. This linear relationship between reflectance and transmittance is predicted by Twersky's multiple-scattering theory,¹¹ and the relationship should remain valid at wavelengths outside the 600–630-nm range tested by Anderson and Sekelj. In addition, the parameters a_1 and a_2 account for the incomplete collection of the back hemisphere, as is the case in the eye. Because measurements were performed for planar slabs of blood, we are not certain that Eq. (7) is valid for light scattered by the cylindrical geometry of blood in a retinal vessel. However, we are unaware of any analytical models of light transport in blood that are capable of modeling this cylindrical geometry. Future efforts might explore a Monte Carlo simulation of photon transport through this cylindrical geometry and verify those results through scattering measurements.

Using Eq. (7) as an expression for the backscattered reflectance, we rewrite Eq. (6) as

$$\begin{aligned} \Phi_v = & \alpha R_f \Phi_0 \exp(-\epsilon cd) + \beta R_f \Phi_0 \exp(-2\epsilon cd) + a_1 \Phi_0 \\ & + a_2 \Phi_0 \exp(-\epsilon cd). \end{aligned} \quad (8)$$

Using Eqs. (2), (3), and (4), we can now write the transmittance of a retinal vessel as

$$\begin{aligned} T_v = & \left(\alpha + \frac{a_2}{R_f} \right) \exp\{-[s\epsilon_{\text{HbO}_2} + (1-s)\epsilon_{\text{Hb}}]cd\} \\ & + \beta \exp\{-2[s\epsilon_{\text{HbO}_2} + (1-s)\epsilon_{\text{Hb}}]cd\} + \frac{a_1}{R_f}. \end{aligned} \quad (9)$$

Equation (9) addresses the primary light paths that contribute to a retinal oxygen saturation measure-

ment. Unfortunately, to calculate oxygen saturation s from Eq. (9) requires that values for seven variables (s , cd , α , β , R_f , a_1 , and a_2) be determined. It is important to note that the ocular fundus reflectivity R_f does not cancel out of this expression for vessel transmittance, explaining why some investigators have needed to include R_f in their retinal oximetry calculations. Although values for R_f can be determined directly from retinal scans, it is unlikely that the remaining parameters could be determined from a least-squares regression to multiwavelength transmittance measurements. In addition, the parameters α , β , R_f , a_1 , and a_2 are expected to be functions of wavelength.

Because it is unlikely that Eq. (9) could be applied directly to measured transmittance data, it is useful to explore the expected magnitudes of the parameters of Eq. (9) to determine which terms, if any, can be neglected. Subsections 3.C and 3.D present approximations to Eq. (9) that may prove more manageable for calculating oxygen saturation.

C. Negligible Backscattering Approximation

Equation (9) simplifies considerably if the effects of light that is directly backscattered by RBC's into the oximeter can be neglected. Backscattering can be neglected if $a_1/R_f \ll 1$ and $a_2/R_f \ll 1$. Measurements made on the optic disk (where fundus reflectivity is highest) or measurements made with green wavelengths (where backscattering is lowest because of high hemoglobin absorption) represent possible situations in which backscattering might be negligible. We have not experimentally verified these hypotheses, but present the equations as a starting point for future investigations.

In the absence of backscattering, Eq. (9) reduces to

$$T_v = \alpha \exp(-\epsilon cd) + \beta \exp(-2\epsilon cd). \quad (10)$$

In the cases of double-pass transmission ($\alpha = 0$) or single-pass transmission ($\beta = 0$), Eq. (10) reduces to the form of the traditional oximetry equation, Eq. (1). In general, however, this reduction is not possible. In theory, the four parameters α , β , s , and cd could be determined by one measuring the vessel transmittance at four or more wavelengths. In practice, the nonlinear regression that is required to determine these four parameters proves difficult. However, a further level of simplification is often possible.

Taking the negative logarithm of Eq. (10), we obtain the expression

$$D_v = -\ln[\alpha \exp(-\epsilon cd) + \beta \exp(-2\epsilon cd)]. \quad (11)$$

Equation (11) cannot be simplified further, but performing a series expansion about ϵcd , we obtain

$$\begin{aligned} D_v = & -\ln(\alpha + \beta) + \frac{\alpha + 2\beta}{\alpha + \beta} \epsilon cd - \frac{\alpha\beta}{2(\alpha + \beta)^2} (\epsilon cd)^2 \\ & + O[(\epsilon cd)^3]. \end{aligned} \quad (12)$$

To determine how many orders of this expansion must be considered, the values of ϵcd , α , and β must

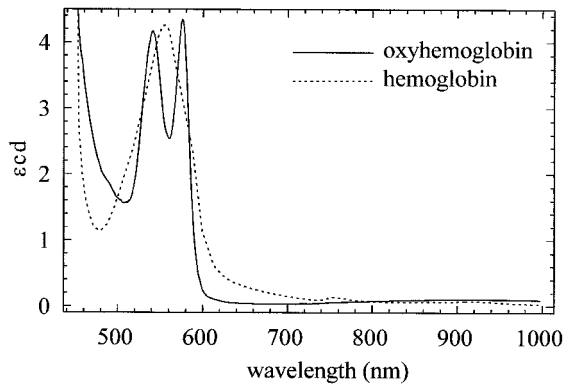


Fig. 4. Values of ϵcd for a typical retinal vessel, where vessel diameter $d = 150 \mu\text{m}$ and the hemoglobin concentration $c = 15 \text{ g/dl}$. Absorption coefficient data are from Ref. 21.

be known. We assume a value for retinal diameter to be $d = 150 \mu\text{m}$ and a hemoglobin concentration of $c = 15 \text{ g/dl}$. Figure 4 shows the anticipated values of ϵcd given the known values of ϵ for hemoglobin and oxyhemoglobin from 450 to 1000 nm (the safe wavelength range useful for retinal vessel oximetry).

We know that $0 \leq \alpha \leq 1$, $0 \leq \beta \leq 1$, and $\alpha + \beta \leq 1$. Measurements performed by our research group indicate that β is significantly smaller than α for our instrumentation, meaning that single-pass transmission and backscattered light are the dominant collected light path.²⁷ The Monte Carlo simulation by Hammer *et al.*²⁰ predicts that the double-pass contribution is significantly smaller than the single-pass contribution for all typical retinal vessel diameters. Choosing a value of β to be 0.10, we can show that the second-order and higher terms of Eq. (12) still contribute as much as 10% to the D_v series for values $\epsilon cd > 2$ (wavelengths less than $\sim 595 \text{ nm}$). However, for $\epsilon cd < 0.5$ (wavelengths between ~ 625 and 1000 nm), these higher-order terms typically contribute less than 1% to the total summation. Therefore, for wavelengths longer than 625 nm, or for sufficiently small vessels (less than $50 \mu\text{m}$ in diameter), we write Eq. (12) as

$$D_v = -\ln(\alpha + \beta) + \frac{\alpha + 2\beta}{\alpha + \beta} \epsilon cd. \quad (13)$$

The vessel transmittance can then be written as

$$T_v = (\alpha + \beta) \exp \left[-\epsilon \left(\frac{\alpha + 2\beta}{\alpha + \beta} \right) cd \right]. \quad (14)$$

This expression has the same form as the traditional vessel oximetry equation, Eq. (1), where $T_s = \alpha + \beta$, and $\chi = (\alpha + 2\beta)/(\alpha + \beta)$. Appropriately, these terms have the limits $0 \leq T_s \leq 1$ and $1 \leq \chi \leq 2$.

The wavelength dependence of α and β are unknown, but it is reasonable to expect that they will be nearly constant over small wavelength ranges. Over larger spectral ranges, α and β likely must be expressed as functions of wavelength, requiring that T_s and χ be functions of wavelength. The traditional

oximetry equation, Eq. (1), includes this wavelength dependence of T_s ; however, the factor χ in Eq. (1) must also be a function of wavelength (except in the limiting cases $\alpha \rightarrow 0$ or $\beta \rightarrow 0$). To date, no reported attempts at retinal vessel oximetry have included this wavelength dependence of χ .

D. Negligible Double-Pass Approximation

It is possible that the double-pass component of the signal collected by a retinal vessel oximeter is negligible (i.e., $\beta \ll \alpha$). The Monte Carlo simulation by Hammer *et al.*²⁰ predicts that the collected double-pass flux is the smallest component in retinal vessel oximetry and that Φ_{dp} may be negligible for vessels larger than $\sim 160 \mu\text{m}$. If the double-pass component can be ignored, then the general oximetry equation, Eq. (9), can be written as

$$T_v = \left(\alpha + \frac{a_2}{R_f} \right) \exp(-\epsilon cd) + \frac{a_1}{R_f}. \quad (15)$$

Equation (15) contains an additive term a_1/R_f that is not present in the traditional oximetry equation, Eq. (1). The existence of this term has not been reported previously, and we expect that including this term in retinal oximetric calculations could improve the accuracy of these measurements. The fundus reflectivity R_f remains as a term in Eq. (15); however, measurements of R_f can be made directly by the oximeter instrumentation. If the wavelength dependencies of α , a_1 , and a_2 are assumed to be minimal (across sufficiently small wavelength ranges), then the five parameters (s , cd , α , a_1 , and a_2) might be determined from a regression to multiwavelength transmittance measurements. More likely, the wavelength dependence of α , a_1 , and a_2 will need to be better understood so that broader wavelength ranges can be used.

It is interesting to explore a first-order expansion of Eq. (15) as was done in Subsection 3.C. In this case, T_v is found to be

$$T_v = \left(\alpha + \frac{a_1 + a_2}{R_f} \right) \exp \left(-\frac{a_2 + \alpha R_f}{a_1 + a_2 + \alpha R_f} \epsilon cd \right) \quad (16)$$

for small values of ϵcd . This expression has a form similar to the traditional oximetry equation, Eq. (1), where

$$T_s(\lambda) = \alpha + \frac{a_1 + a_2}{R_f}, \quad (17)$$

$$\chi(\lambda) = \frac{a_2 + \alpha R_f}{a_1 + a_2 + \alpha R_f}. \quad (18)$$

Some observations can be made about the magnitudes of T_s and χ . For very low values of fundus reflectivity ($R_f \ll 1$), the scattering transmittance can become greater than one ($T_s > 1$). In the case of a perfectly absorbing retinal background ($R_f = 0$), the typical vessel profile of Fig. 3 would instead show an increase in collected flux at the center of the vessel.

More importantly, T_s will be dependent on wavelength because of the wavelength dependence of R_f .

Perhaps the most important observations regarding Eq. (16) relate to the parameter χ . It is shown that χ can be strongly dependent on wavelength (because of the wavelength dependence of R_f). This has the effect of a path length through the sample that varies with wavelength. In addition, $\chi < 1$ for all possible values of α , R_f , a_1 , and a_2 , resulting in a reduced path length that could be detrimental to oxygen saturation sensitivity. Through a better understanding of the backscattering terms (a_1 and a_2), we expect to determine how small χ could become.

E. Summary

The equations in this paper were developed to explain the results from two different experiments performed by our group. These experiments are considered separately below. We found that simplified versions of Eqs. (14) or (16) work well in our experiments. Both of these equations can be simplified to the form

$$T_v(\lambda) = T_s(\lambda)\exp[-\chi(\lambda)cd\varepsilon(\lambda)]. \quad (19)$$

Another equation that appears promising for experimental work is a simplified version of Eq. (15):

$$T_v(\lambda) = T_s(\lambda)\exp[-\varepsilon(\lambda)cd] + g(\lambda). \quad (20)$$

We have not yet successfully applied Eq. (20) to our experimental data.

4. Experimental Results

A. *In Vivo* Calibration of a Scanning Laser Oximeter

We have previously reported the successful *in vitro* calibration of a scanning laser retinal vessel oximeter¹³ called the eye oximeter (EOX). This instrument scans four laser beams (629, 678, 821, and 899 nm) into the eye and collects the returned flux as the beams are scanned across a retinal vessel. The *in vitro* calibration was performed in a model eye consisting of whole human blood pumped through a micropipette that was embedded in index-matched fluid. A plano-convex lens simulated the cornea and lens of the eye, and a 4-mm-thick slab of Spectralon (Labsphere, Inc. North Sutton, N.H.) simulated the scattering layers of the ocular fundus. Spectralon provides extremely diffuse, high reflectance that is spectrally neutral across our wavelength range. Using the traditional oximetry equation, Eq. (1), we obtained a good calibration by selecting a wavelength dependence for $T_s(\lambda)$ that increases linearly by 3% over the wavelength range 629–899 nm. We performed this by fitting the equation

$$T_v(\lambda) = T_s f(\lambda)\exp\{-\chi cd[s\varepsilon_{\text{Hb}}(\lambda) + (1-s)\varepsilon_{\text{HbO}_2}(\lambda)]\} \quad (21)$$

to the transmittance data, where the three unknowns are the oxygen saturation s , the product χcd , and a constant scattering transmittance T_s . The correc-

tion factor $f(\lambda)$ is a linear function that increases from 1.00 at 629 nm to 1.03 at 899 nm.

Our next step in calibrating this instrument was to measure a retinal artery in an anesthetized swine during graded hypoxia. All animal protocols were approved by the Institutional Animal Care and Use Committee of the University of Alabama at Birmingham and followed Public Health Service guidelines regarding the care and use of laboratory animals. The oxygen administered to the swine was decreased in a stepwise manner. At each oxygen level, arterial oxygen saturation from the femoral artery was measured with a CO-oximeter and a retinal artery was scanned with the EOX. Retinal measurements were acquired near the optic disk, and it is assumed that retinal and femoral arterial saturations are equal. Twelve saturation levels were measured, ranging from 36% O₂ saturation to 95% O₂ saturation.

Figure 5 shows the result of our applying the model eye calibration, Eq. (21), to the swine measurements. The top graph displays the regressed values of oxygen saturation versus the known arterial saturations. Although the correlation between actual saturation and calculated retinal saturation is quite strong ($r^2 = 0.958$), there is a systematic offset in the calculated saturations that results in low saturations being measured significantly too high. The bottom graph of Fig. 5 shows the results of the regression. The filled data points are the measured vessel transmittances for the 36% O₂ saturation measurement, and the open data points are for the 95% O₂ saturation measurement. The dashed curve is the spectra calculated by Eq. (21) when the regressed values of s , χcd , and T_s are used. It can be seen that Eq. (21) fits the transmittance data quite well, even though the regressed saturation values are incorrect.

The appearance of the scans acquired from the model eye and from the eye of the swine were extremely similar. The only significant difference between the scans was the reflectance of the ocular fundus R_f . The Spectralon background used in the model eye is spectrally neutral and highly reflective. In the swine, R_f was relatively high at 899 nm, where hemoglobin and melanin absorb weakly, but was approximately 10% as reflective at 629 nm because of higher hemoglobin and melanin absorption. Unfortunately, at the time the measurements were made, it was believed that R_f did not affect our measurements. As such, we did not measure Φ_0 and cannot accurately quantify the reflectance of the swine fundus. Nevertheless, because of the obvious wavelength variation of R_f in the swine, we believe that selecting different values for the wavelength dependence of scattering $f(\lambda)$ was justified.

We developed an algorithm to search for values of $f(\lambda)$ that yielded the optimum *in vivo* calibration using Eq. (21). Figure 6 displays the results of this calibration by use of the scattering factors $f(629) = 0.990$, $f(670) = 1.010$, $f(821) = 0.965$, and $f(899) = 1.000$. A piecewise cubic interpolating polynomial was applied to these values to facilitate plotting. As can be seen in the top graph of Fig. 6, a good calibra-

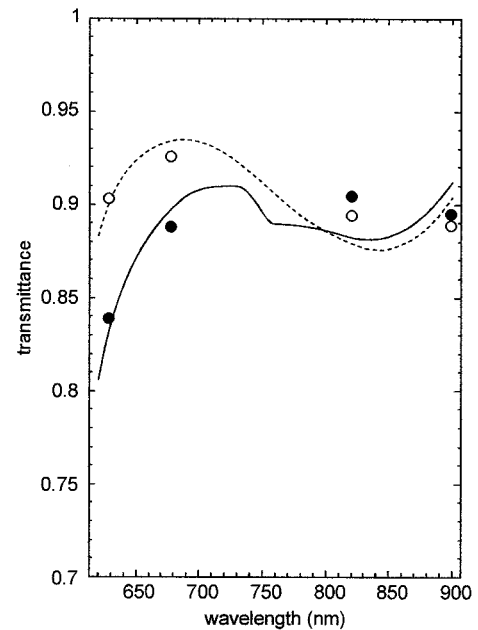
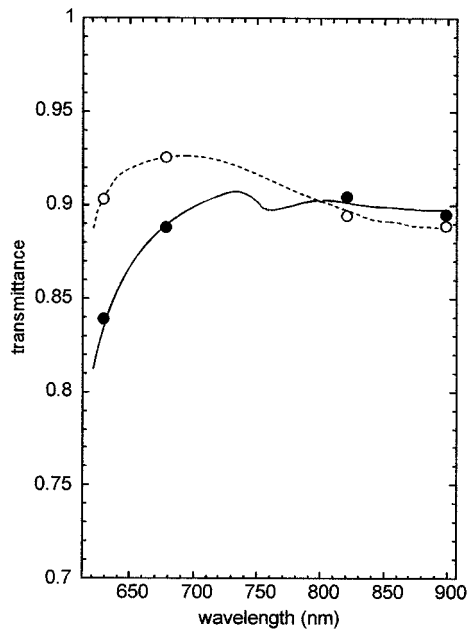
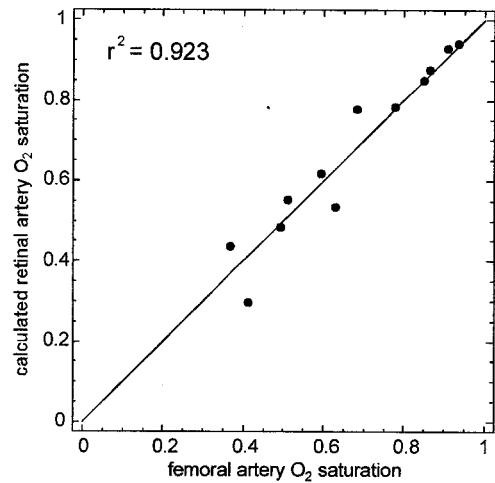
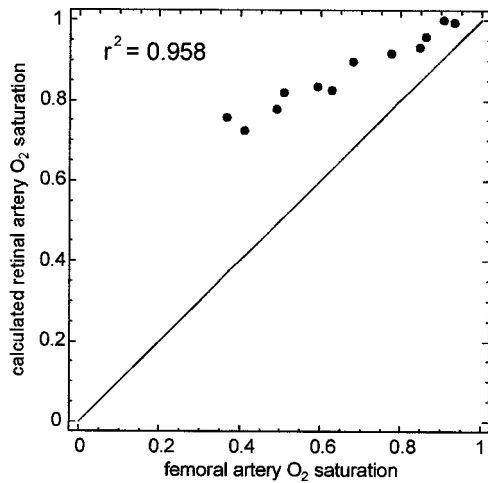


Fig. 5. Application of the model eye calibration equation to the *in vivo* swine data. The top graph compares the calculated retinal arteria saturation with the measured femoral artery oxygen saturation. The bottom graph displays the resulting best-fit spectra. The filled circles are measured vessel transmittances for a femoral artery saturation of 36% O₂ saturation, and the open circles are for 95% O₂ saturation.

Fig. 6. Application of the wavelength-dependent scattering equation, Eq. (21), to the *in vivo* swine data. The best-fit scattering factors $f(\lambda)$ were found to be $f(629) = 0.990$, $f(670) = 1.010$, $f(821) = 0.965$, and $f(899) = 1.000$.

tion ($r^2 = 0.923$) was obtained and no systematic offset was observed between the actual femoral artery saturation and the calculated retinal arterial saturation. The bottom graph of Fig. 6 demonstrates that although the regressed saturation values were correct, the model function, Eq. (21), does not provide a good fit to the transmittance data. As such, this calibration attempt is considered unsuccessful. Note that whereas only two saturation values are shown in the bottom graph of Fig. 6, these two curves are representative of the entire family of curves obtained by Eq. (21). No values of $f(\lambda)$ could be found that provided both correct saturation calcu-

lations and an acceptable fit to the transmittance data.

The inability of the wavelength-dependent scattering model of Eqs. (1) and (21) to describe our *in vivo* measurements led to the development of the oximetry equations presented in this paper. Because changes in fundus reflectivity R_f appear to affect our measurement, we cannot justify use of the negligible backscattering approximation. However, we found that the first-order expansion of the negligible double-pass approximation of Eq. (16) offers some improvement to our calibration. At present, we have made no attempt to quantify values for the wavelength-dependent parameters α , a_1 , a_2 , and R_f of Eq. (16). Instead, we reduce these parameters into $\chi(\lambda)$ and $T_s(\lambda)$. As a final simplification, we assume

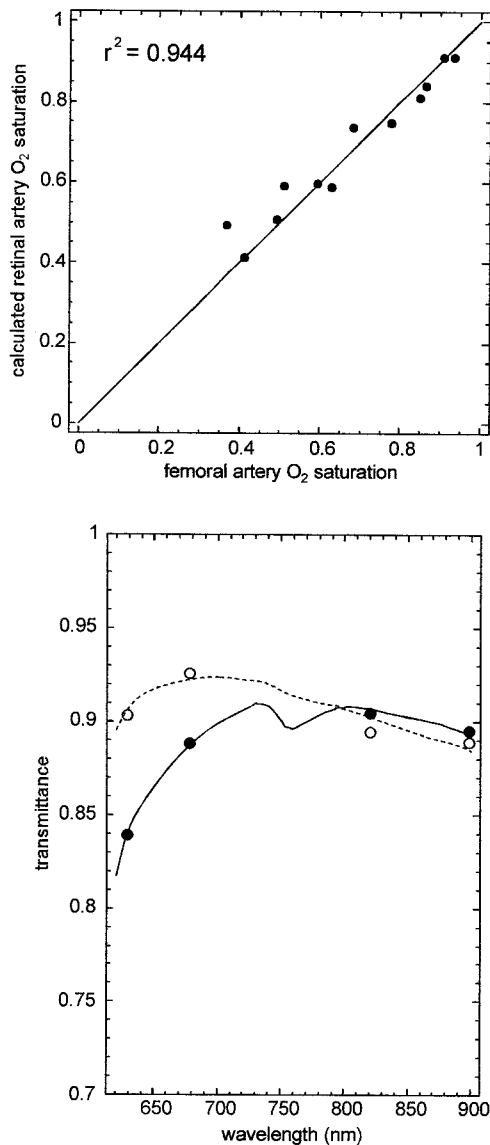


Fig. 7. Application of the wavelength-dependent path-length equation, Eq. (22), to the *in vivo* swine data. The best-fit path-length factors $\chi(\lambda)$ were found to be $\chi(629) = 0.65$, $\chi(670) = 0.7$, $\chi(821) = 0.85$, and $\chi(899) = 1.00$.

that the wavelength dependence of $\chi(\lambda)$ is more significant than that of $T_s(\lambda)$, and we therefore assume that $T_s(\lambda)$ is a constant. We fit the resulting equation

$$T_v(\lambda) = T_s \exp\{-\chi(\lambda)cd[s\epsilon_{\text{HbO}_2}(\lambda) + (1-s)\epsilon_{\text{Hb}}(\lambda)]\} \quad (22)$$

to our measured transmittance data, where s , cd , and T_s are the unknowns and values of $\chi(\lambda)$ are selected to provide the optimum calibration.

Figure 7 contains the results of this calibration by use of the optimum χ values: $\chi(629) = 0.65$, $\chi(670) = 0.7$, $\chi(821) = 0.85$, and $\chi(899) = 1.00$. Analysis of Fig. 7 reveals that Eq. (21) results in both accurate calculated arterial saturations ($r^2 = 0.944$) and an

acceptable fit to the measured transmittance data. As such, allowing a wavelength-dependent χ value while holding T_s constant produced an acceptable calibration for this experiment. To the best of our knowledge, this is the first time such an equation has been applied to vessel oximetry.

It is interesting to note that the optimum values of χ were found to decrease as the reflectivity of the fundus decreased at shorter wavelengths (because of increased hemoglobin and melanin absorption).¹⁸ This behavior is predicted by Eq. (18). Note that the optimum values of $\chi(\lambda)$ can be scaled by an arbitrary constant; however, the resulting cd product from a regression will scale inversely by the arbitrary constant, thus maintaining the same value of $\chi(\lambda)cd$. As such, the fact that these optimum values of $\chi(\lambda)$ are less than 1 does not necessarily imply the reduced path length predicted by the negligible double-pass approximation.

Finally, the data presented here were acquired from a single location on the retina of one swine. Studies with additional animals are ongoing, and preliminary results indicate that use of Eq. (20) leads to an improved calibration compared with use of the traditional oximetry equation, Eq. (1). However, we find that optimum values of $\chi(\lambda)$ tend to vary between subjects. We are working to quantify this variation and attempting to find relationships between $\chi(\lambda)$ and the fundus reflectivity and vessel diameter.

B. *In Vitro* Calibration of a Confocal Scanning Laser Oximeter

We are currently developing a confocal scanning laser EOX called the EOX-2.²⁸ This instrument operates like a confocal scanning laser ophthalmoscope²⁹ and produces a live video image of a subject's retina acquired at 830 nm. To acquire a spectroscopic data set, the EOX-2 cycles through up to six lasers. In this study, the EOX-2 was equipped with three diode lasers (635, 670, and 830 nm) and a fiber-coupled argon-ion laser (488 nm). This wavelength combination was selected based on a previous study that predicts reduced errors in the calculated saturation.⁸ These lasers are interlaced into a single video frame that is digitized at 10-bit resolution. The transmittance of the vessel is measured at each wavelength, and the oxygen saturation is calculated from these transmittances.

The confocal detection path of the EOX-2 significantly reduces the collection of light that is reflected or scattered from nonretinal planes such as the cornea and crystalline lens. In addition, the confocal arrangement should limit the collected light paths to the directly backscattered flux Φ_{bs} and double-pass transmitted flux Φ_{dp} .

Using the model eye described in Subsection 4.A, we measured five blood samples ranging from 11% O₂ saturation to 100% O₂ saturation with the EOX-2. The hemoglobin concentration of the samples was 13.9 g/dl and, a 270- μm pipette (inner diameter) was used to simulate the retinal blood vessel.

Because it had worked well in previous model eye

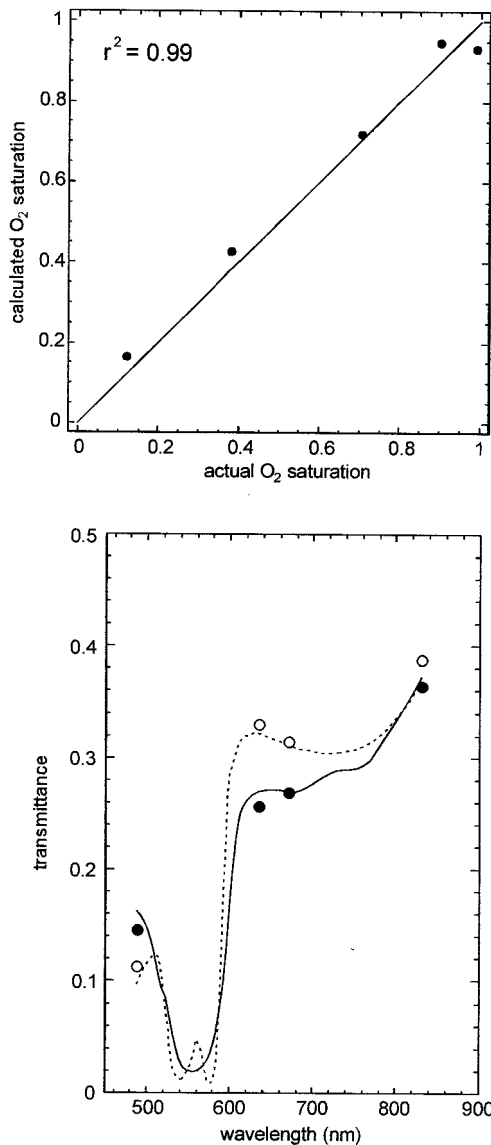


Fig. 8. Calibration of the confocal scanning laser oximeter in a model eye. The top graph compares the calculated oxygen saturation with the actual saturation of the known whole-blood samples. The bottom graph displays the resulting best-fit spectra. The filled circles are measured vessel transmittances for an oxygen saturation of 11% O₂ saturation, and the open circles are for 100% O₂ saturation.

calibration experiments, we used the traditional oximetry equation, Eq. (21), to calculate s , χcd , and T_s . The calibration procedure involved an iterative technique to determine optimum values for the wavelength-dependent scattering factors $f(\lambda)$. We found that the values $f(488) = 1.000$, $f(635) = 0.919$, $f(670) = 0.892$, and $f(830) = 1.000$ resulted in an excellent calibration. The results of this study are shown in Fig. 8. The correlation between the actual oxygen saturation and the calculated saturation was extremely strong ($r^2 = 0.99$); however, only five data points were present. In addition, the model function fit the transmittance data well.

Although this study demonstrates that accurate

oxygen saturation values can be calculated *in vitro*, it is also interesting to examine the regressed values of χcd . Because the values $c = 13.9$ g/dl and $d = 270$ μm were known, we could determine an absolute value of χ . We found that $\chi = 0.22$ for this data set. Although a value of $\chi < 1$ seems counterintuitive, this result was predicted by the negligible double-pass approximation. The reduced path length is a direct consequence of the backscattering of light by RBC's. The factor a_1 in Eq. (7) shows that as ecd approaches infinity, the light backscattered by the blood column does not approach zero, even though the transmitted flux does approach zero. This results in the apparent path-length reduction that we experimentally measure.

5. Discussion and Conclusions

Our group has monitored changes in retinal vessel oxygen saturation,^{5,6,30} and recently we have demonstrated an accurate *in vitro* calibration.¹³ Yet after significant advancements in instrumentation, wavelength selection, and signal processing, we have not obtained consistently accurate calibrations in a swine model. The difficulties of *in vivo* calibration led to the development of the improved oximetry equations presented here. The complete retinal vessel oximetry equation, Eq. (9), contains too many terms to be useful in a measurement; however, more manageable expressions are obtained through some simplifying approximations. In this paper we explored the negligible double-pass and negligible backscattering approximations. Further investigation is required to determine the validity of these approximations; however, one of the resulting simplified expressions, Eq. (19), has been shown to provide a better model to *in vivo* data than the traditional oximetry equation, Eq. (1).

Although Eqs. (19) and (20) both appear promising for retinal vessel oximetry, both equations contain wavelength-dependent factors that are likely to be functions of fundus reflectivity, and are possibly functions of vessel diameter, retinal position (because of varying thickness of the retinal layers), and hemoglobin concentration. Monte Carlo simulations of light interaction with the retina²⁰ should provide a theoretical framework for determining the relationships between these parameters; however, a large database of vessel saturation measurements acquired across a range of known oxygen saturations, hemoglobin concentration, retinal position, fundus pigmentations, and vessel diameters will eventually be required if we are to definitively show calibrated measurements from a retinal vessel oximeter.

This study emphasizes one of the trade-offs that must be considered in the development of a retinal vessel oximeter. A recent study by Smith⁸ predicts that several discrete wavelengths ranging from 488 to 905 nm can be selected that offer the highest sensitivity to oxygen saturation across a range of vessel diameters. To use this large wavelength range, however, the wavelength dependence of the unknown parameters in Eqs. (19) and (20) will need to be well

understood. The choice of three closely spaced green wavelengths, as used by Delori,³ minimizes the wavelength dependence of these unknown parameters, perhaps allowing constant values to be used. These wavelengths, however, also result in decreased sensitivity to oxygen saturation.⁸ Although it is not clear which approach will ultimately lead to well-calibrated retinal vessel oxygen saturation measurements, understanding the light paths that comprise the measurement will be critical to the success of the technique. We expect that the equations developed here will prove beneficial to future retinal vessel oximetry investigations, regardless of the wavelengths selected or instrumentation used for performing the measurements.

The authors thank J. E. Drewes and L. C. Heaton for their help in collecting and analyzing the data presented here. We gratefully acknowledge the financial support for this research by the U.S. Army Medical Research and Materials Command and by the Office of Naval Research.

References and Notes

- J. B. Hickam, R. Frayser, and J. C. Ross, "A study of retinal venous blood oxygen saturation in human subjects by photographic means," *Circulation* **27**, 375–385 (1963).
- A. J. Cohen and R. A. Laing, "Multiple scattering analysis of retinal blood oximetry," *IEEE Trans. Biomed. Eng.* **23**, 391–400 (1976).
- F. C. Delori, "Noninvasive technique for oximetry of blood in retinal vessels," *Appl. Opt.* **27**, 1113–1125 (1988).
- D. Schweitzer, L. Leistritz, M. Hammer, M. Seibor, U. Bartsch, and J. Strobel, "Calibration-free measurement of the oxygen saturation in retinal vessels of men," in *Ophthalmic Technologies V*, J.-M. Parel, Q. Ren, and K. M. Joos, eds., *Proc. SPIE* **2393**, 210–218 (1995).
- K. R. Denninghoff, M. H. Smith, R. A. Chipman, L. W. Hillman, P. M. Jester, C. E. Hughes, F. Kuhn, and L. W. Rue, "Retinal large vessel oxygen saturation correlates with early blood loss and hypoxia in anesthetized swine," *J. Trauma* **43**, 29–34 (1997).
- M. H. Smith, K. R. Denninghoff, L. W. Hillman, and R. A. Chipman, "Oxygen saturation measurements of blood in retinal vessels during blood loss," *J. Biomed. Opt.* **3**, 296–303 (1998).
- J. S. Tiedeman, S. E. Kirk, S. Srinivas, and J. M. Beach, "Retinal oxygen consumption during hyperglycemia in patients with diabetes without retinopathy," *Ophthalmology* **105**, 31–36 (1998).
- M. H. Smith, "Optimum wavelength selection for retinal vessel oximetry," *Appl. Opt.* **38**, 258–267 (1999).
- J. M. Beach, K. J. Schwenzler, S. Srinivas, and J. S. Tiedeman, "Oximetry of retinal vessels by dual-wavelength imaging: calibration and influence of pigmentation," *J. Appl. Physiol.* **86**, 748–758 (1999).
- O. W. Van Assendelft, *Spectrophotometry of Haemoglobin Derivatives* (Thomas, Springfield, Ill., 1970).
- V. Twersky, "Absorption and multiple scattering by biological suspensions," *J. Opt. Soc. Am.* **60**, 1084–1093 (1970).
- R. N. Pittman and B. R. Duling, "A new method for the measurement of percent oxyhemoglobin," *J. Appl. Physiol.* **38**, 315–320 (1975).
- J. J. Drewes, M. H. Smith, K. R. Denninghoff, and L. W. Hillman, "An instrument for the measurement of retinal vessel oxygen saturation," in *Optical Diagnostics of Biological Fluids IV*, A. V. Priezzhev, M. V. Lomonosov, and T. Asakura, eds., *Proc. SPIE* **3591**, 114–120 (1999).
- R. A. MacRae, J. A. McClure, and P. Latimer, "Spectral transmission and scattering properties of red blood cells," *J. Opt. Soc. Am.* **51**, 1366–1372 (1961).
- A. G. Borovoi, E. I. Naats, and U. G. Opper, "Scattering of light by a red blood cell," *J. Biomed. Opt.* **3**, 364–372 (1998).
- M. Hammer, D. Schweitzer, B. Michel, E. Thamm, and A. Kolb, "Single scattering by red blood cells," *Appl. Opt.* **37**, 7410–7418 (1998).
- F. C. Delori, E. S. Gragoudas, and R. C. Pruett, "Monochromatic ophthalmoscopy and fundus photography: the normal fundus," *Arch. Ophthalmol. (Chicago)* **95**, 861–868 (1977).
- F. C. Delori and K. P. Pflibsen, "Spectral reflectance of the human ocular fundus," *Appl. Opt.* **28**, 1061–1077 (1989).
- I. J. Hodgkinson, P. B. Greer, and A. C. B. Molteno, "Point-spread function for light scattered in the human ocular fundus," *J. Opt. Soc. Am. A* **11**, 479–486 (1994).
- M. Hammer, S. Leistritz, L. Leistritz, D. Schweitzer, E. Thamm, and K. H. Donnerhacke, "Monte Carlo simulation of retinal vessel profiles for the interpretation of *in vivo* oximetric measurements by imaging fundus reflectometry," in *Medical Applications of Lasers in Dermatology, Ophthalmology, Dentistry, and Endoscopy*, G. B. Altshuler, R. Birngruber, M. Dal Forte, R. Hibst, H. Hoenigsmann, N. Krasner, and F. Laffitte, eds., *Proc. SPIE* **3192**, 211–218 (1997).
- S. Prahla has compiled data of hemoglobin extinction coefficients from several investigators. The data are available at <http://omlc.ogi.edu/spectra/hemoglobin/index.html>.
- N. M. Anderson and P. Sekelj, "Light-absorbing and scattering properties of nonhemolysed blood," *Phys. Med. Biol.* **12**, 173–184 (1967).
- N. M. Anderson and P. Sekelj, "Reflection and transmission of light by thin films of nonhaemolysed blood," *Phys. Med. Biol.* **12**, 185–192 (1967).
- J. M. Steinke and A. P. Shepherd, "Diffusion model of the optical absorbance of whole blood," *J. Opt. Soc. Am. A* **5**, 813–822 (1988).
- V. Twersky, "Absorption and multiple scattering by biological suspensions," *J. Opt. Soc. Am.* **60**, 1084–1093 (1970).
- A. N. Yaroslavsky, I. V. Yaroslavski, T. Goldbach, and H.-J. Schwarmaier, "Influence of the scattering phase function approximation on the optical properties of blood determined from the integrating sphere measurements," *J. Biomed. Opt.* **4**, 47–53 (1999).
- J. J. Drewes, "Four wavelength retinal vessel oximetry," Ph.D. dissertation (University of Alabama, Huntsville, Ala., 1999).
- A. Lompo, "A confocal scanning laser ophthalmoscope for retinal vessel oximetry," Ph.D. dissertation (University of Alabama, Huntsville, Ala., 1999).
- R. H. Webb, G. W. Hughes, and F. C. Delori, "Confocal scanning laser ophthalmoscope," *Appl. Opt.* **26**, 1492–1499 (1987).
- K. R. Denninghoff, M. H. Smith, R. A. Chipman, L. W. Hillman, P. M. Jester, F. Kuhn, D. Redden, and L. W. Rue, "Retinal venous oxygen saturation correlates with blood volume," *Acad. Emerg. Med.* **5**, 577–582 (1998).